Electronic Supplementary Material (ESI) for Energy & Environmental Science.

Crystalline Nickel, Cobalt, and Manganese Antimonates as Electrocatalysts for the Chlorine Evolution Reaction

Ivan A. Moreno-Hernandez[1], Bruce S. Brunschwig[2], Nathan S. Lewis[1,2,3]

[1]Division of Chemistry and Chemical Engineering, 127-72, California Institute of Technology, Pasadena, CA 91125, USA

[2]Beckman Institute Molecular Materials Research Center, California Institute of Technology, Pasadena, CA 91125, USA

[3]Kavli Nanoscience Institute, California Institute of Technology, Pasadena, CA 91125, USA

*Correspondence to: nslewis@caltech.edu

Supplementary Information

Materials and Methods

Chemicals

All chemicals were used as received, including antimony(III) chloride ($SbCl_3$, Alfa Aesar, ACS, 99.0% min), tin(IV) chloride hydrate ($SnCl_4 \cdot xH_2O$, Alfa Aesar, 98%), sodium chloride (NaCl, Macron Chemicals, ACS grade), potassium iodide (KI, EMD Millipore, ACS grade), sodium thiosulfate pentahydrate ($Na_2S_2O_3$, Alfa Aesar, ACS grade), 1.0 M hydrochloric acid (1.0 M HCl(aq), Fluka Analytical), multielement standard solution 1 for ICP (Sigma Aldrich, TraceCERT), sulfuric acid (H_2SO_4(aq), Fischer Scientific, TraceMetal grade, 93-98%), sodium hydroxide (NaOH, Macron Chemicals, ACS grade), antimony standard for ICP (Sigma Aldrich, TraceCERT), potassium chloride (KCl, Macron Chemicals, ACS grade), and gallium-indium eutectic (Alfa Aesar, 99.99%). Deionized water with a resistivity of 18.2 MΩ-cm was obtained from a Millipore deionized water system.

Sample Preparation

A previously described spray pyrolysis procedure was used to deposit conductive films of antimony-doped tin oxide (ATO).[1, 2] The process consisted of spraying a 0.24 M $SnCl_4$ solution in ethanol doped with 3 mol% $SbCl_2$ onto a quartz microscope slide heated at 550 °C on a hot plate. The thickness of the ATO film was adjusted by controlling the duration of the spray. ATO films with a sheet resistance of 5- 10 Ω sq^{-1}, as determined from four-point probe measurements, were used for subsequent experiments.

Metallic films of Ni, Co, Mn, Sb, $NiSb_2$, $CoSb_2$, and $MnSb_2$ were deposited onto the ATO substrates with an AJA Orion sputtering system. The ATO substrates were partially

covered with Kapton tape to prevent complete coverage of the ATO with the catalyst films, to form a direct contact between the ATO and the working electrode wire. The metallic films were co-sputtered from four metallic targets in an Ar plasma: Antimony (ACI Alloys, 99.95%), Nickel (ACI Alloys, 99.95%), Cobalt (ACI Alloys, 99.95%), and Manganese (ACI Alloys 99.95%). The chamber pressure was < 10^{-7} Torr prior to the depositions. A chamber pressure of 5 mTorr was sustained during the depositions with an Ar flow rate of 20 sccm. The samples were not intentionally heated during the deposition process. The power applied to the metal targets was varied to obtain similar transition metal loadings and a stoichiometry close to 2:1 Sb:M in MSb_x samples. The actual stoichiometry and loading of Ni, Co, Mn, and Sb was determined by dissolving in 1.0 M H_2SO_4(aq) films deposited on glass, and then using the concentration of the metals as determined by ICP-MS, the areas of the samples dissolved, and the amount of H_2SO_4(aq) used during the dissolution to obtain the total loading.

After the metal films were deposited on ATO, the films were annealed in a muffle furnace (Thermolyne F48020-80) to form the crystalline oxides.[2] Unless otherwise specified, the temperature was increased to 750 °C at a ramp rate of 10 °C min^{-1}, was held at 750 °C for 6 h, and then allowed to return to room temperature without active cooling. $RuTiO_x$ films with the same molar loading (~ 1.5 μmol cm^{-2}) as the MSb_2O_x films were prepared by drop casting 4 μL cm^{-2} of a 0.11 M $RuCl_3$ and 0.26 M $TiCl_4$ solution in ethanol onto ATO, followed by drying on a hot plate at 400 °C.[3] The $RuTiO_x$ was annealed at 500 °C for 1 h in a muffle furnace.[3] The samples were cleaved into pieces that had exposed ATO regions, and In-Ga eutectic was scribed on the ATO. The electrode support consisted of a tinned Cu wire that was threaded through a glass tube. The Cu wire was coiled and bonded to the ATO substrate by use of Ag paint (SPI, Inc). The contact was allowed to dry for at least 2 h at room temperature or for 15 min at 85 °C

in an oven. Hysol 9460 epoxy was used to insulate the Cu, ATO, and In-Ga from the electrolyte and to define the geometric electrode area. The epoxy was allowed to cure for > 12 h at room temperature or for 2 h at 85 °C in an oven. The electrode area and a calibration ruler was imaged with an optical scanner (Epson Perfection V360), and the electrode area was quantified with ImageJ software. Electrode areas were between 1 and 40 mm^2 unless otherwise specified.

Materials Characterization

X-ray diffraction (XRD) data were collected with a Bruker D8 Discover instrument. The Cu Kα (1.54 Å) x-ray beam was generated with a tube current of 1000 μA and a tube voltage of 50 kV, and was detected with a Vantec-500 2-dimensional detector. The incident beam was collimated with a 0.5 mm diameter mono-capillary collimator. A calibrated visible laser was used to align the sample with the x-ray beam. XRD data were collected in coupled θ-2θ mode, with four scans collected every 20° from a 2θ theta range of 20° – 80°. The x-ray radiation was collected for 1 h for each scan, corresponding to 4 h per sample. The 2-dimensional signal was integrated to obtain a 1-dimensional scan with an angular resolution of 0.01° 2θ. The x-ray diffraction peaks were analyzed using Bruker EVA software with reference patterns of SnO_2 for the ATO substrate, in addition to reference patterns for monoclinic Sb_2O_4, orthorhombic Sb_2O_4, $NiSb_2O_6$, $CoSb_2O_6$, $MnSb_2O_6$, RuO_2 and TiO_2 obtained from the Crystallography Open Database or literature.[4, 5] Scanning-electron microscopy (SEM) images were collected using immersion mode with an accelerating voltage of 10 kV on a Nova nanoSEM 450 (FEI) instrument.

X-ray Photoelectron Spectroscopy

X-ray photoelectron spectroscopy (XPS) scans were collected using a Kratos Axis NOVA (Kratos Analytical, Manchester, UK) at a background pressure of $<10^{-9}$ Torr. The x-ray

source consisted of a monochromatic Al kα beam with an energy of 1486.6 eV. Survey scans were collected at 1.0 eV resolution, and high-resolution scans were collected at 0.05 eV resolution. The binding energy of the scans was corrected against the adventitious C 1s peak with a constant offset to obtain an adventitious C 1s peak energy of 284.8 eV. The M 2p spectra of Ni, Co, and Mn were fit using previously reported fitting parameters.[6] The reported peak separations, FWHM ratios, and relative peak areas were used to fit the collected M 2p spectra. However, in most cases the peak shapes could not be fit adequately without shifting the peaks towards more positive binding energies. Since MSb_2O_x samples are chemically different than MO_x or $M(OH)_2$ samples, we tentatively assign the shifted peak shapes to M(II) in a MSb_2O_6 lattice. For example, while the peak position of $NiSb_2O_x$ is similar to other Ni(II) species, the peak shape could not be adequately fit with Ni 2p spectra of Ni oxide or hydroxide species. We introduced an addition peak shape that consisted of the $Ni(OH)_2$ spectra shifted 1.0 eV more positive.[7] We tentatively assign this peak shape to Ni(II) in the $NiSb_2O_6$ lattice. The XP spectrum of Sb $3d_{3/2}$ was used to determine the oxidation state of the surface Sb on MSb_2O_x samples. Literature values of Sb $3d_{3/2}$ peak binding energies for oxidation states of 3^+, $3^+/5^+$, and 5^+ are 539.5 eV, 540.1 eV, and 540.4 eV respectively, for a C 1s peak binding energy of 284.8 eV.[8]

Electrochemical Testing

NaCl was used to make 4.0 M aqueous solutions, and 1 M HCl(aq) was used to adjust the pH to 2 as measured by a pH probe. A saturated calomel electrode (SCE) was calibrated with a normal hydrogen electrode (NHE). The NHE consisted of a platinum disk (CH Instruments) submerged in a H_2 saturated 1.0 M sulfuric acid electrolyte, with $H_2(g)$ bubbled underneath the Pt disk to ensure saturation. The potential of the SCE was 0.244 V vs. NHE. Electrochemical measurements were collected in a two-compartment cell with the compartments separated using

a Nafion N424 membrane. The cathode compartment was filled with 0.1 M NaOH(aq), and the anode compartment was filled with 4.0 M NaCl(aq) adjusted to pH = 2 with HCl(aq). After 48 h chronopotentiometry experiments, the pH of the electrolyte was usually 2.05 – 2.10. The OER acidifies solutions, and the observations are consistent with the observed increase in pH arising from minor leakage of NaOH through the Nafion N424 membrane. The electrolyte was replaced after 48 h to prevent the pH from increasing. The working and reference electrodes were placed in the anode compartment, and the counter electrode was placed in the cathode compartment. The working, reference, and counter electrodes consisted of the sample, an SCE, and a carbon rod or Ni wire, respectively. The anode compartment was saturated with Cl_2(aq) by applying ~ 10 V for at least 30 min between the counter electrode and a second working electrode that consisted of a graphite rod. The saturation of the electrolyte with Cl_2(aq) did not substantially affect the activity of the electrocatalysts or the pH of the electrolyte. However, this step was implemented to establish and maintain a well-defined potential based on the Nernst equation, which requires that Cl_2(aq) is present in the electrolyte. Cyclic voltammograms were collected at a scan rate of 10 mV s^{-1} unless otherwise specified. Electrochemical data were collected using a digital potentiostat (SP-200, Bio-Logic). The thermodynamic potential for chlorine evolution was calculated to be 1.331 V vs. NHE in 4.0 M NaCl(aq).[9]

The roughness factor (RF) of the TMAs was determined by comparing the electrochemically active surface area of bare ATO substrates and TMAs, as determined from impedance measurements. Impedance measurements were collected in 4.0 M NaCl(aq) adjusted to pH = 2 with the electrolyte additionally saturated with Cl_2(aq). Electrodes were held at 1.660 V vs. NHE for 15 s prior to impedance measurements, which were collected at the same potential with a frequency range of 20 Hz – 20 kHz, with a sinusoidal wave amplitude of 10 mV. The

impedance data were fit with a circuit model consisting of a resistor in series with a parallel component consisting of a constant phase element and another resistor.[10] The capacitance was obtained by using a formula previously reported for the analysis of this circuit.[10] The formula is shown below:

$$C_{DL} = \left[Q_0 \left(\frac{1}{R_s} + \frac{1}{R_{CT}} \right)^{(a-1)} \right]^{\frac{1}{a}}$$

Where Q_0 and a are the parameters associated with the constant phase element, R_s is the series resistance, R_{ct} is the charge-transfer resistance, and C_{DL} is the determined double-layer capacitance. The impedance data were fit using EC-Lab software by constraining all variables to positive values, and using the Randomize + Simplex method for at least 10,000 iterations. The fitting process was repeated at least four times to ensure that the best fit was obtained. Table S5 shows examples of impedance data collected for the electrocatalysts studied herein. ATO substrates prepared by a spray deposition method have previously been determined from atomic force microscopy measurements to have a RF = 1.32.[2] The capacitance of ATO electrodes was determined with impedance measurements, and divided by the projected area of the electrodes to determine the geometric-area normalized capacitance. The geometric-area normalized capacitance of ATO was 14.4 ± 1.6 μF cm^{-2}, which corresponds to an electrochemical surface area normalized capacitance of 11 ± 1 μF cm_{ox}^{-2} after dividing by the RF = 1.32 of ATO. The roughness factor of the TMAs was determined by dividing the geometric-area normalized capacitance of the TMAs by the electrochemical surface area normalized capacitance of ATO (11 μF cm_{ox}^{-2}).

Inductively-coupled plasma mass spectrometry

An Agilent 8000 Triple Quadrupole Inductively Coupled Plasma Mass Spectrometer (ICP-MS) system was used to determine the concentration of various ions in aqueous samples. Calibration solutions were prepared by diluting antimony and multielement standard solutions (Sigma Aldrich) with 18.2 MΩ cm resistivity water. The concentration of various ions was determined from a linear fit of the counts per second of each standard solution versus the known concentration. The mass loading of the TMAs was determined by depositing the MSb_2 (M = Ni, Co, Mn) layers on glass slides that were then cut into ~ 1 cm^2 pieces. The projected area of the pieces was determined with a calibrated optical scanner and ImageJ software. The MSb_2 layers were dissolved in 10 mL of 1.0 M H_2SO_4(aq) for > 100 h, and samples from these solutions were diluted with water and analyzed with ICP-MS. The loading of the catalyst layer was determined using the concentration of M and Sb, the volume of 1.0 M H_2SO_4(aq), and the projected area of the MSb_2 layers. The dissolution of species from TMAs films under chlorine evolution conditions was determined by collecting 40 μL samples of electrolyte from a cell operating at 100 mA cm^{-2} with an initial 5 mL volume of 4.0 M NaCl(aq), pH = 2 electrolyte in the anode compartment, and diluting these samples to 5 mL with 18.2 MΩ cm resistivity water. For $RuTiO_x$ samples, 1 mL of the electrolyte was collected from a 7 mL cell, and electrolyte was replenished after every sample was taken. The 1 mL samples were diluted to 10 mL with 18.2 MΩ cm resistivity water. The dissolution studies for $RuTiO_x$ could only be conducted for ~ 20 h, because the expected Ru dissolution product, RuO_4, is a volatile compound that escapes the anode compartment in conjunction with the evolved Cl_2(g), resulting in an underestimate of the Ru dissolution rate.[11] ICP-MS measurements of Ru in the collected samples after 48 h of the initial measurements verified the volatility of the dissolved Ru. The amount of M and Sb lost was determined from the concentration, volume of the cell, and electrode area. The amount of M

and Sb removed from the cell after each sample was collected was taken into account when determining the amount of metals lost over time during chronopotentiometry measurements.

Chlorine Faradaic Efficiency and Oxygen Evolution Reaction Activity

The faradaic efficiency towards chlorine evolution was determined using an established iodometric titration technique.[12-14] A two-compartment cell separated by a Nafion N424 membrane and with an 8 mL anode compartment was used for this study. The anode compartment was completely filled with 4.0 M NaCl(aq), pH = 2 electrolyte. Electrodes consisting of $RuTiO_x$ or TMAs were operated at 100 mA cm^{-2} for 10 minutes. The electrolyte was transferred to a 25 mL Erlenmeyer flask containing 0.3 g of KI, and 0.2 mL of glacial acetic acid was added to the solution. The resulting yellow solution was titrated with 0.01 M NaS_2O_3(aq) using a 10 mL burette, and starch solution was added near the endpoint. This titration method requires 2 mol of NaS_2O_3(aq) per mol of Cl_2(aq). The moles of Cl_2 expected was calculated using the charge passed during the galvanostatic measurement, Faraday's constant (F, 96485.3389 C mol^{-1}), and the electrons required to obtain Cl_2 (2 mol e^- per mol Cl_2). The faradaic efficiency was determined by comparing the moles of Cl_2(aq) detected to the moles of Cl_2 expected. Measurements were also collected for 4.0 M NaCl(aq), pH =2 electrolyte that had not been used for electrochemical measurements as a blank. At least three measurements were collected per electrode. In these experiments, some minor nucleation of bubbles on the epoxy used to encapsulate the electrodes and the Teflon adapter used seal the electrochemical cell was observed. Since only dissolved species are detected by the iodometric technique, the faradaic efficiency measurements represent a lower limit on the Faradaic efficiency of the electrocatalysts studied herein. The generation of Cl_2(aq) was also verified with colorimetric measurements using N,N-diethyl-p-phenylenediamine. The high activity towards chlorine evolution relative to

oxygen evolution was also verified by collecting cyclic voltammograms of $RuTiO_x$ and TMAs in pH = 2 H_2SO_4(aq) electrolyte.

Supplementary Information Figures

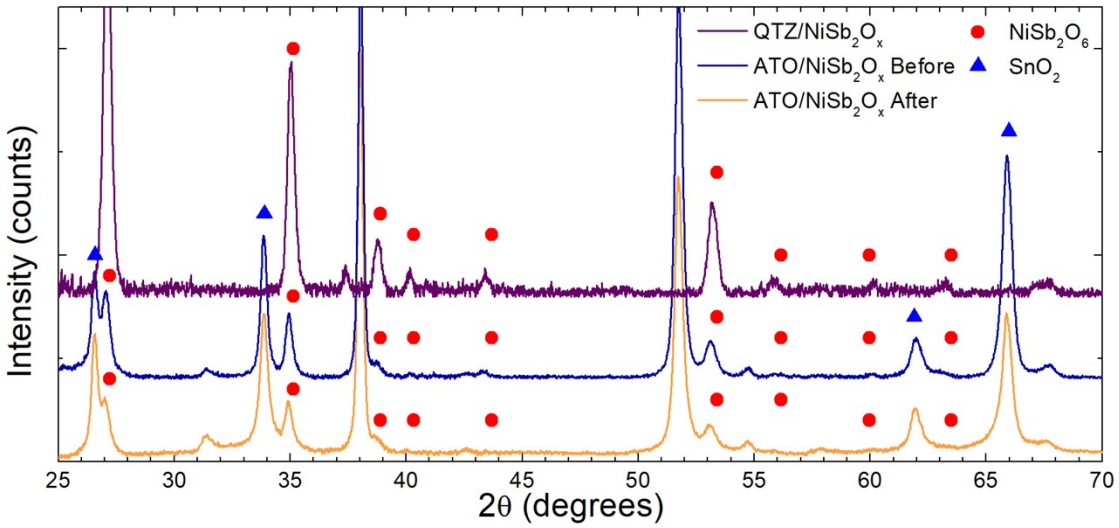

Figure S1. X-ray diffraction of as-synthesized $NiSb_2O_x$ films on quartz and ATO, and $NiSb_2O_x$ films after electrochemical operation in 4.0 M NaCl(aq), pH = 2.0 electrolyte at 100 mA cm^{-2} for 65 h.

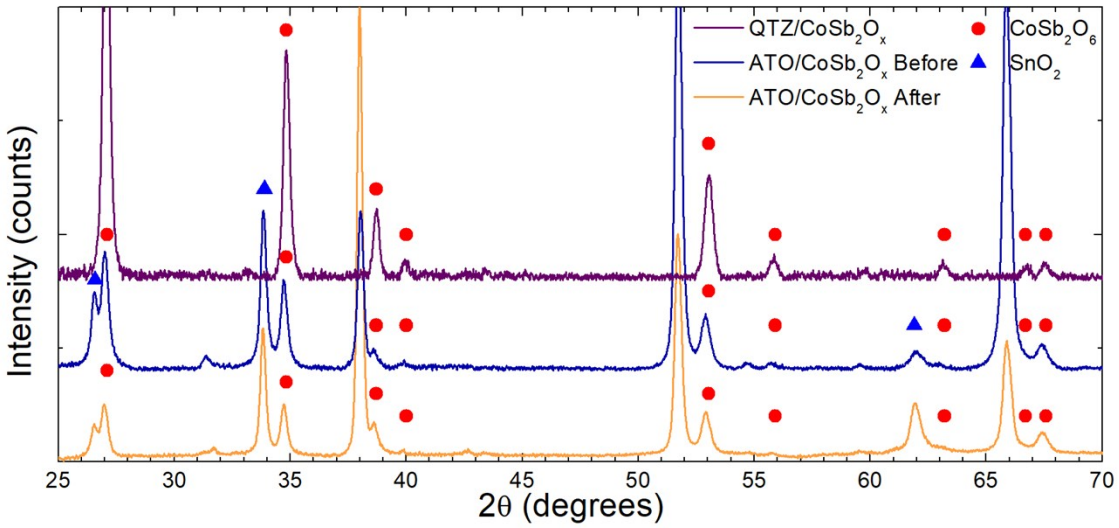

Figure S2. X-ray diffraction of as-synthesized $CoSb_2O_x$ films on quartz and ATO, and $CoSb_2O_x$ films after electrochemical operation in 4.0 M NaCl(aq), pH = 2.0 electrolyte at 100 mA cm^{-2} for 90 h.

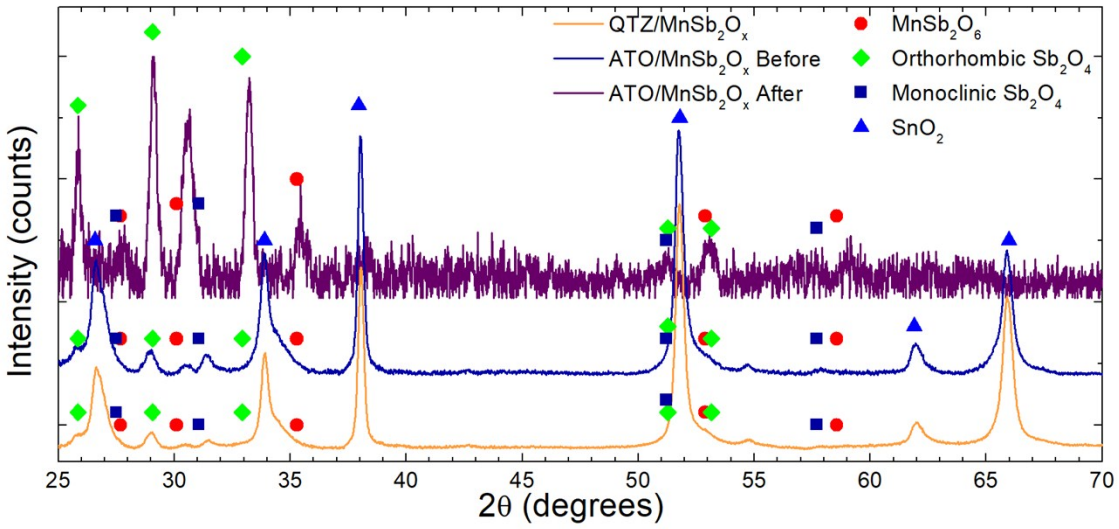

Figure S3. X-ray diffraction of as-synthesized $MnSb_2O_x$ films on quartz and ATO, and $MnSb_2O_x$ films after electrochemical operation in 4.0 M NaCl(aq), pH = 2.0 electrolyte at 100 mA cm^{-2} for 90 h.

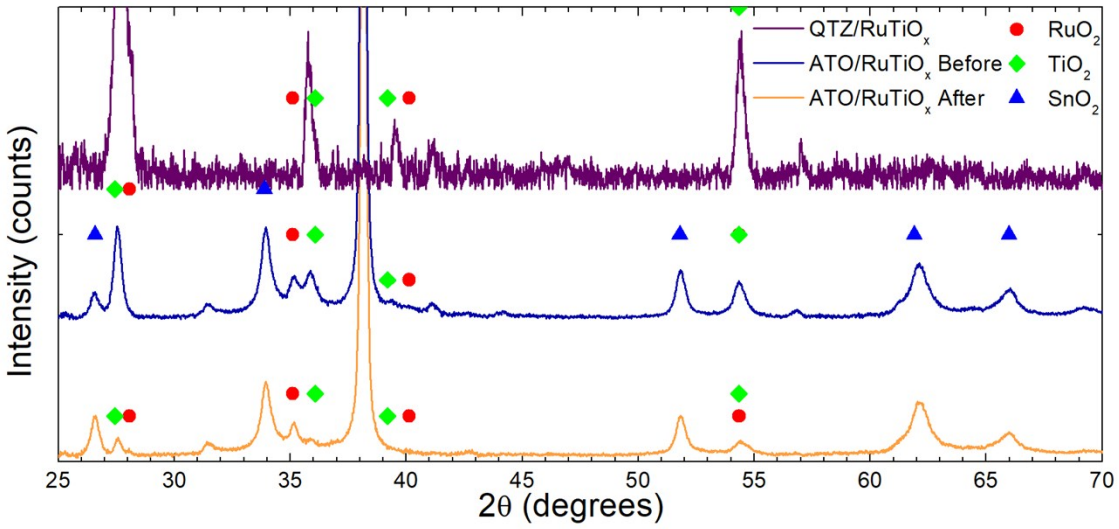

Figure S4. X-ray diffraction of as-synthesized $RuTiO_x$ films on ATO, and $RuTiO_x$ films after electrochemical operation in 4.0 M NaCl(aq), pH = 2.0 electrolyte at 100 mA cm^{-2} for 90 h.

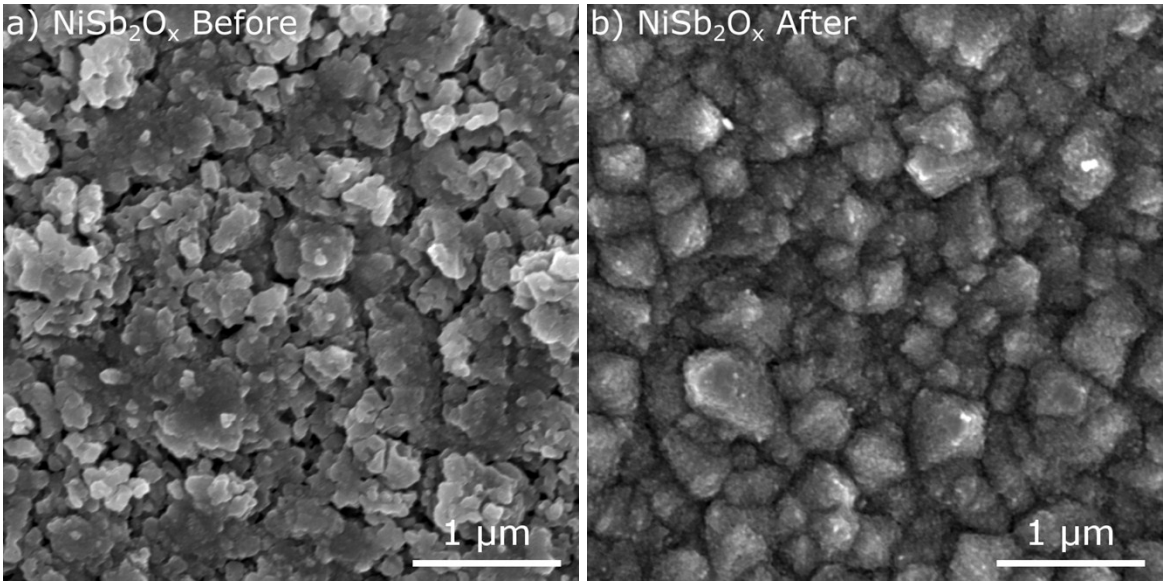

Figure S5. Scanning-electron microscope image of $NiSb_2O_x$: a) before operation, b) after 65 h at 100 mA cm^{-2} in 4.0 M NaCl(aq), pH = 2.0 electrolyte.

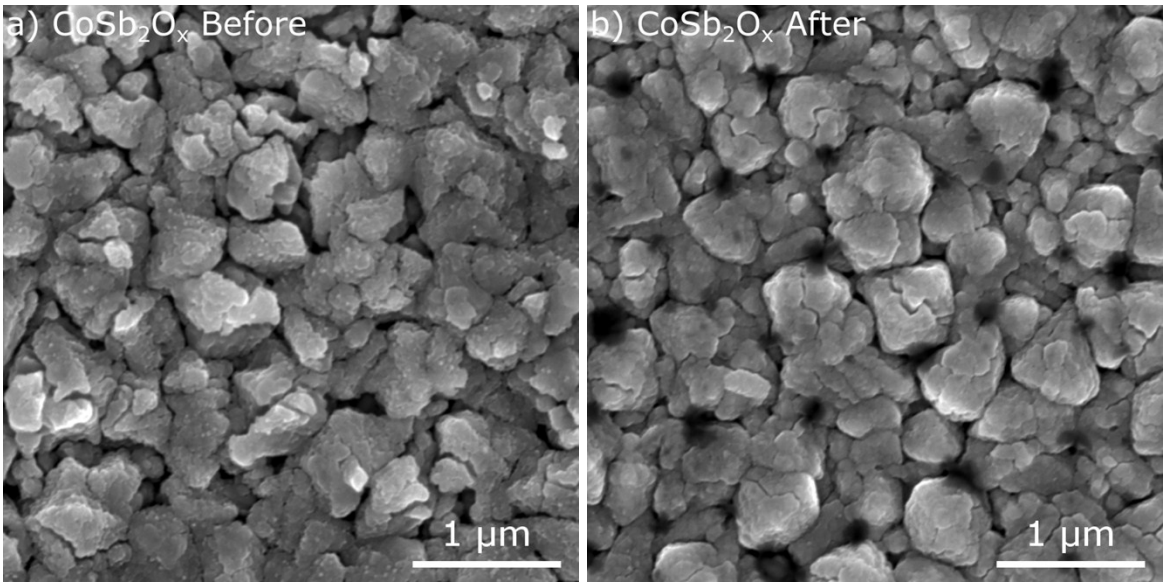

Figure S6. Scanning-electron microscope image of $CoSb_2O_x$: a) before operation, b) after 90 h at 100 mA cm^{-2} in 4.0 M NaCl(aq), pH = 2.0 electrolyte.

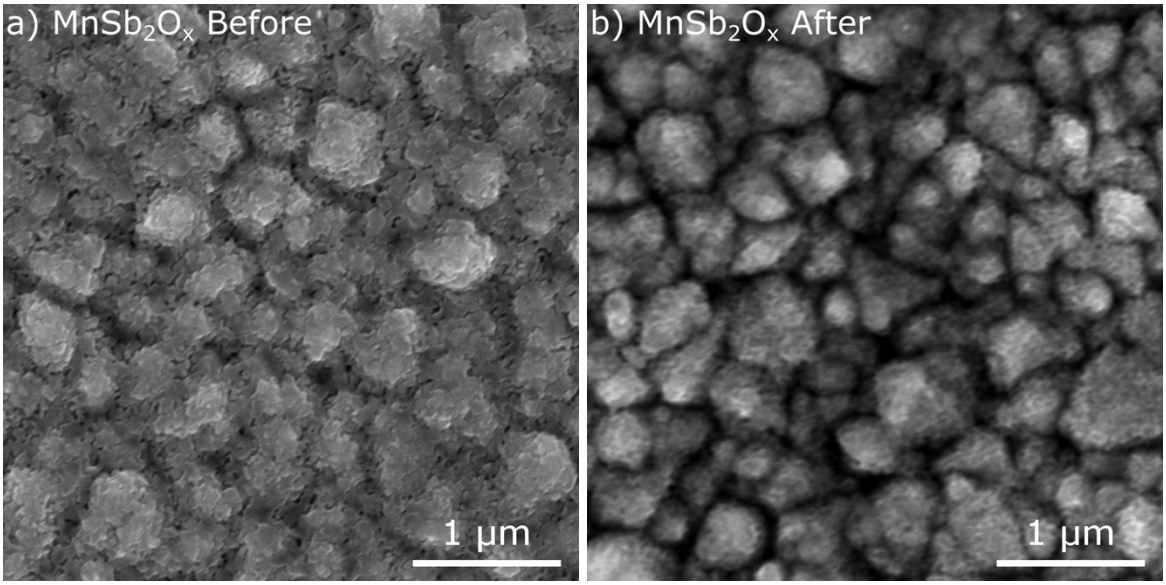

Figure S7. Scanning-electron microscope image of $MnSb_2O_x$: a) before operation, b) after 90 h at 100 mA cm^{-2} in 4.0 M NaCl(aq), pH = 2.0 electrolyte.

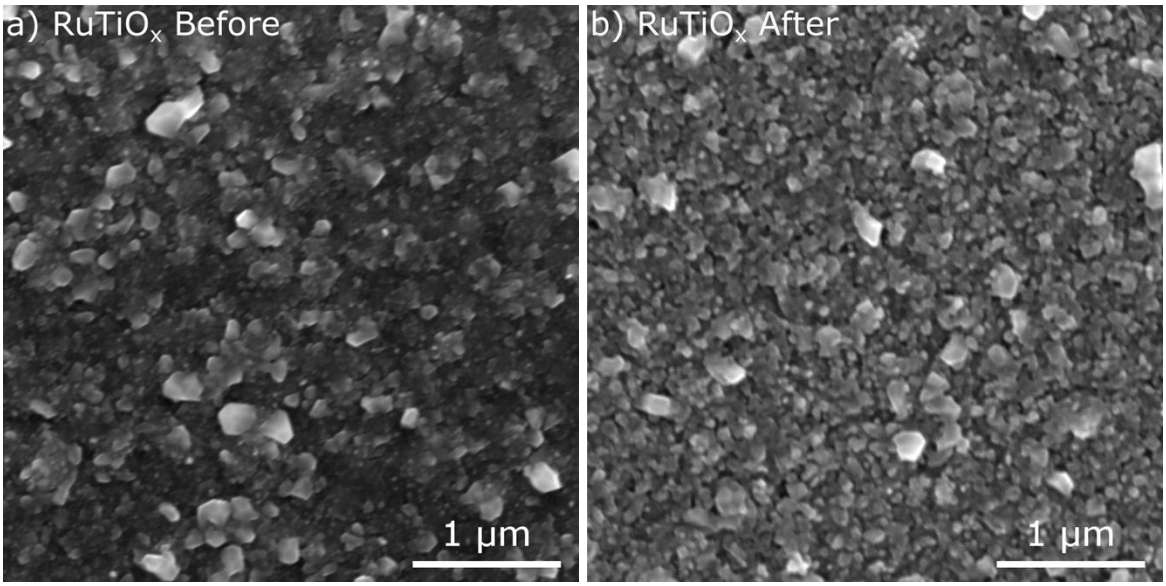

Figure S8. Scanning-electron microscope image of $RuTiO_x$: a) before operation, b) after 90 h at 100 mA cm^{-2} in 4.0 M NaCl(aq), pH = 2.0 electrolyte.

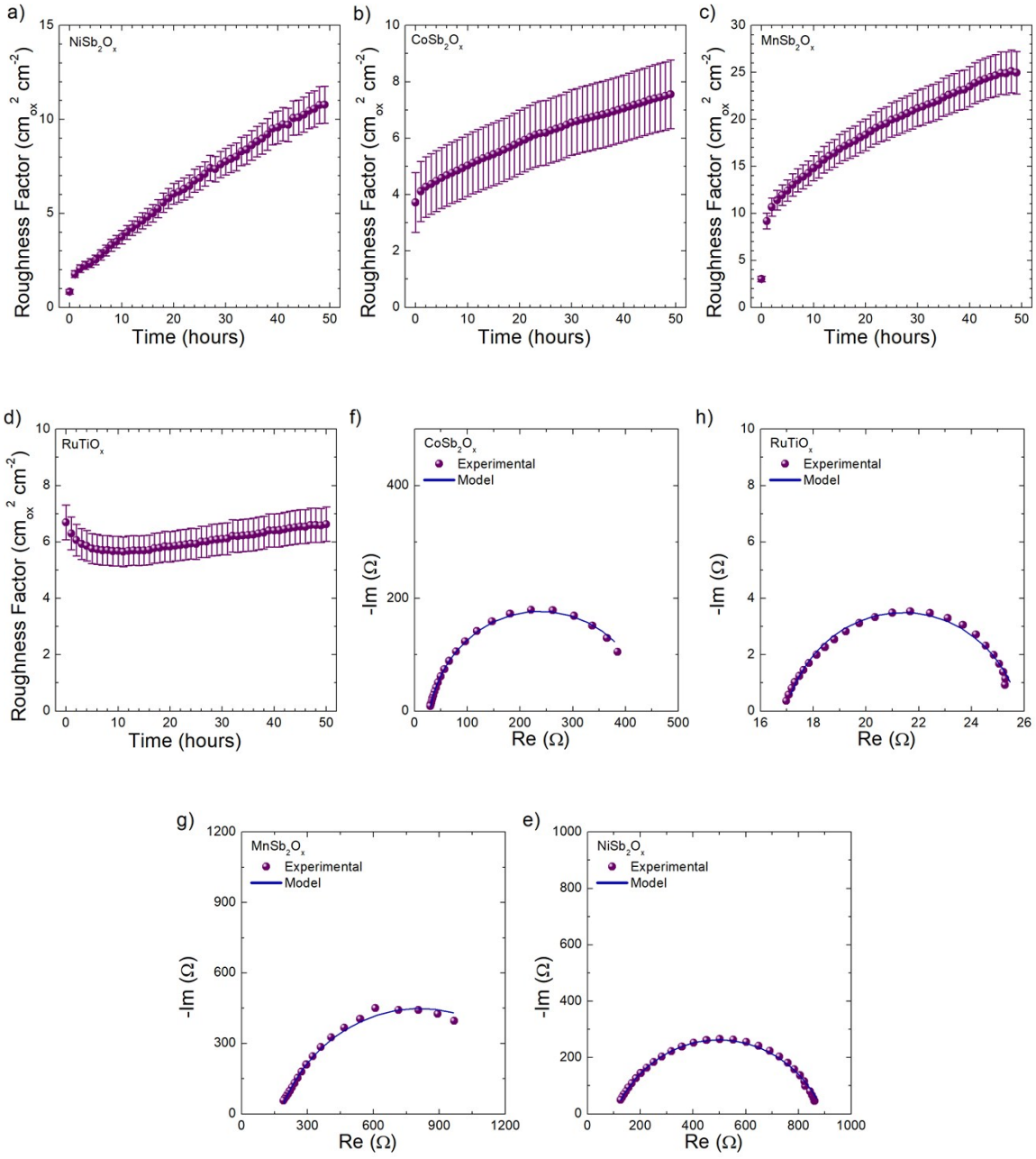

Figure S9. Roughness factor determined from impedance data collected at 1 h intervals between chronopotentiomery stability tests at 100 mA cm^{-2} for a) $NiSb_2O_x$, b) $CoSb_2O_x$, c) $MnSb_2O_x$, and

d) $RuTiO_x$. Comparison between initial impedance data and impedance model fit for e) $NiSb_2O_x$, f) $CoSb_2O_x$, g) $MnSb_2O_x$, and h) $RuTiO_x$.

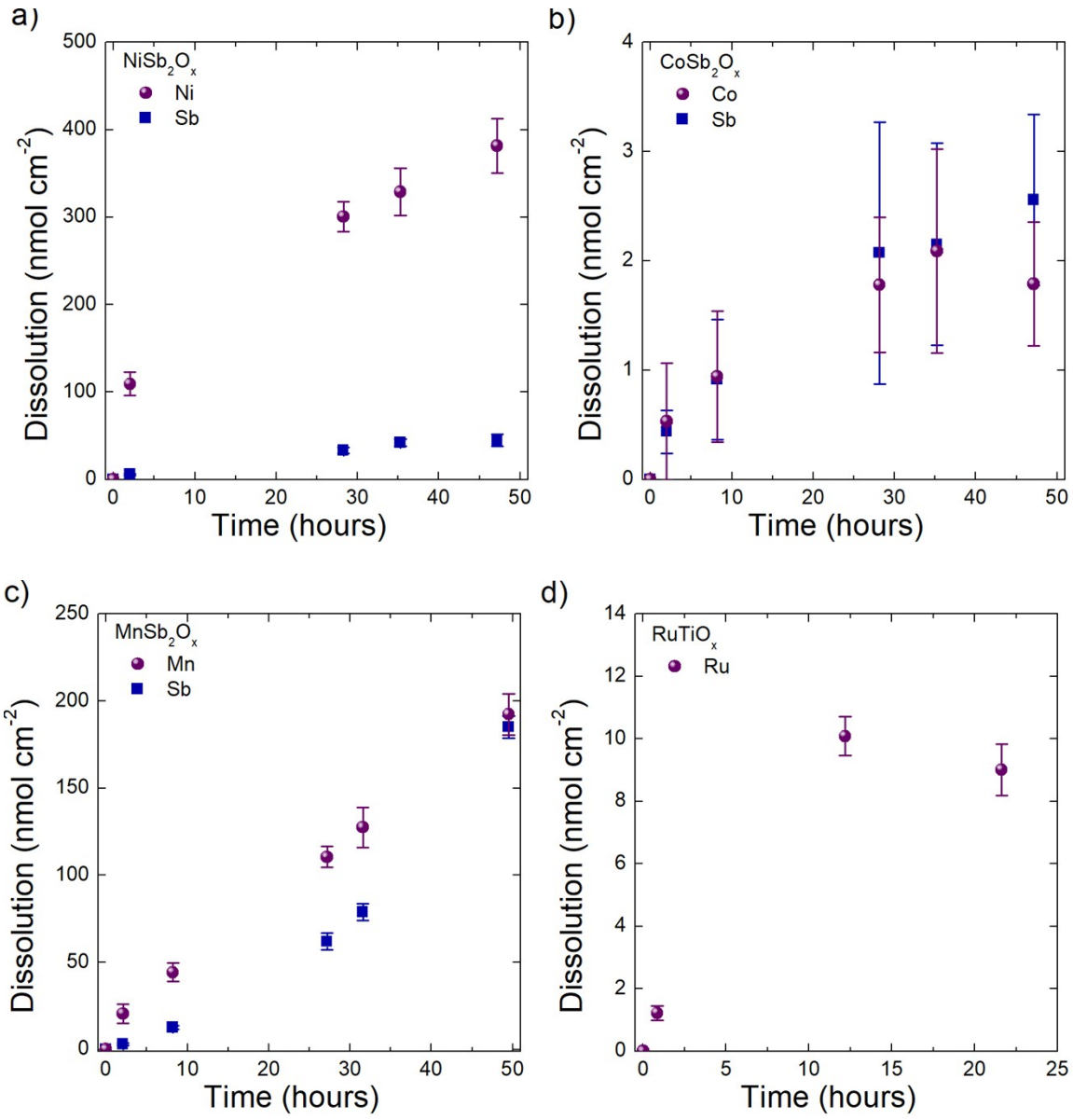

Figure S10. Amount of elements dissolved from MSb_2O_x and $RuTiO_x$ electrodes operated at 100 mA cm^{-2} in 4.0 M NaCl, pH = 2.0 electrolyte: a) $NiSb_2O_x$, b) $CoSb_2O_x$, c) $MnSb_2O_x$, d) $RuTiO_x$.

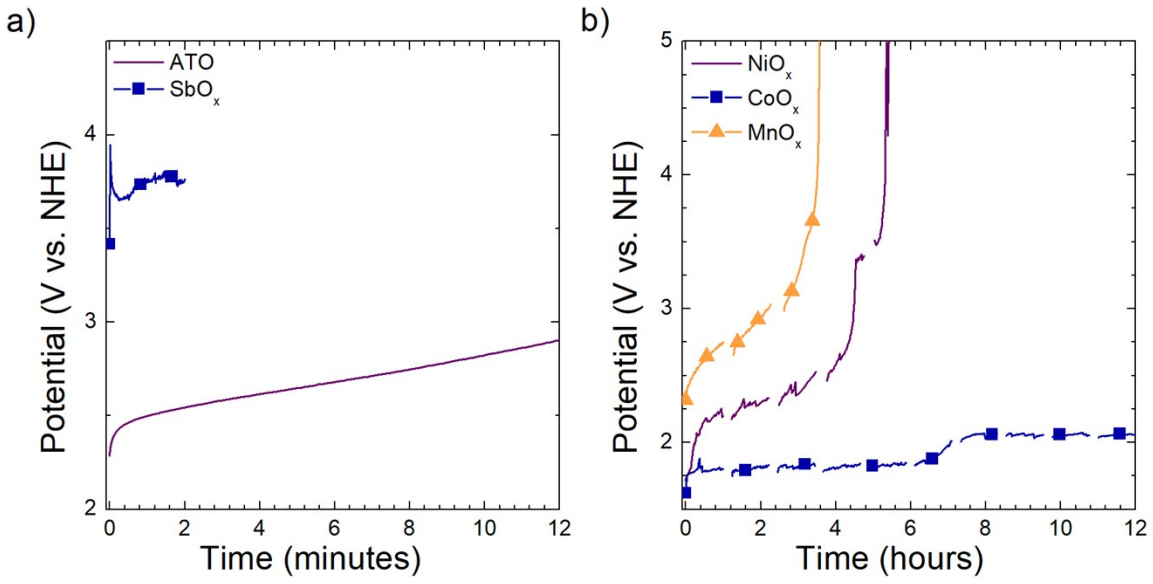

Figure S11. a) Chronopotentiometry of ATO and SbO_x at 100 mA cm^{-2}. b) Chronopotentiometry of NiO_x, CoO_x, and MnO_x at 100 mA cm^{-2}.

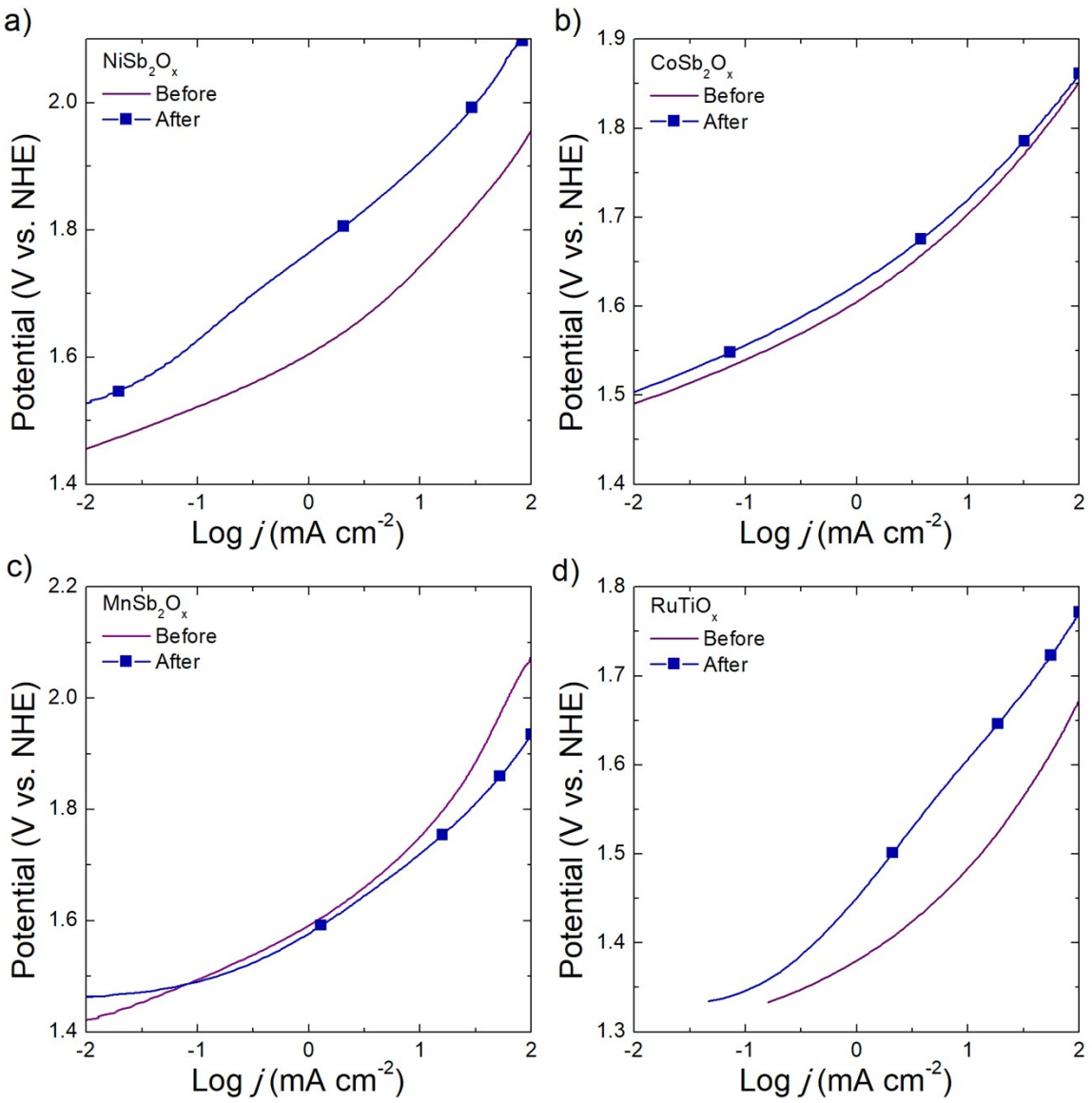

Figure S12. Tafel plots from 10^{-2} to 10^{2} mA cm^{-2} before and after 50 h at 100 mA cm^{-2} for a) $NiSb_2O_x$, b) $CoSb_2O_x$, c) $MnSb_2O_x$, d) $RuTiO_x$. The current-voltage data was collected from cyclic voltammograms.

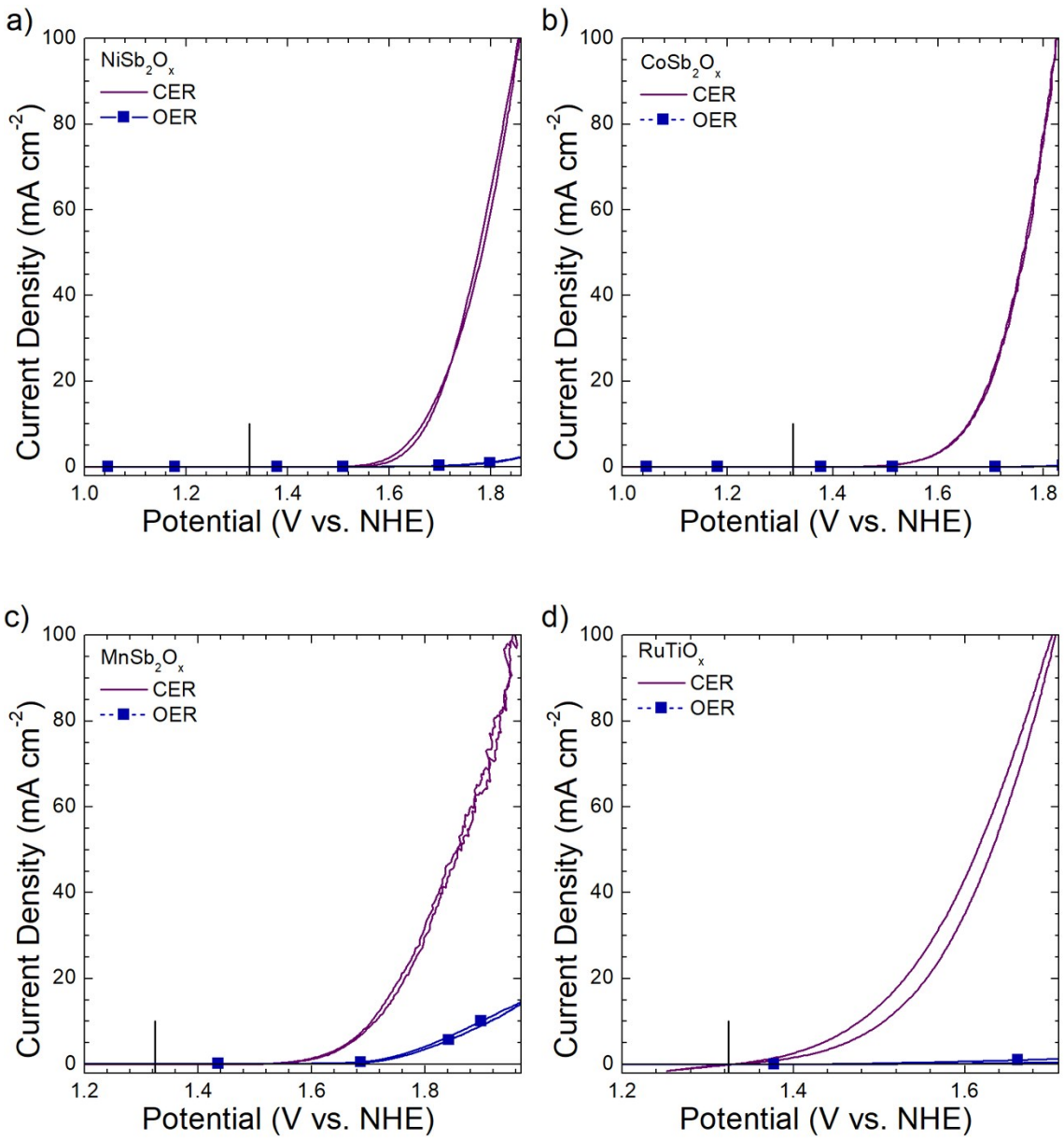

Figure S13. Cyclic voltammograms collected under chlorine evolution conditions [4.0 M NaCl(aq), pH = 2.0] and oxygen evolution conditions [pH = 2.0 H_2SO_4(aq)] for a) $NiSb_2O_x$, b) $CoSb_2O_x$, c) $MnSb_2O_x$, and d) $RuTiO_x$.

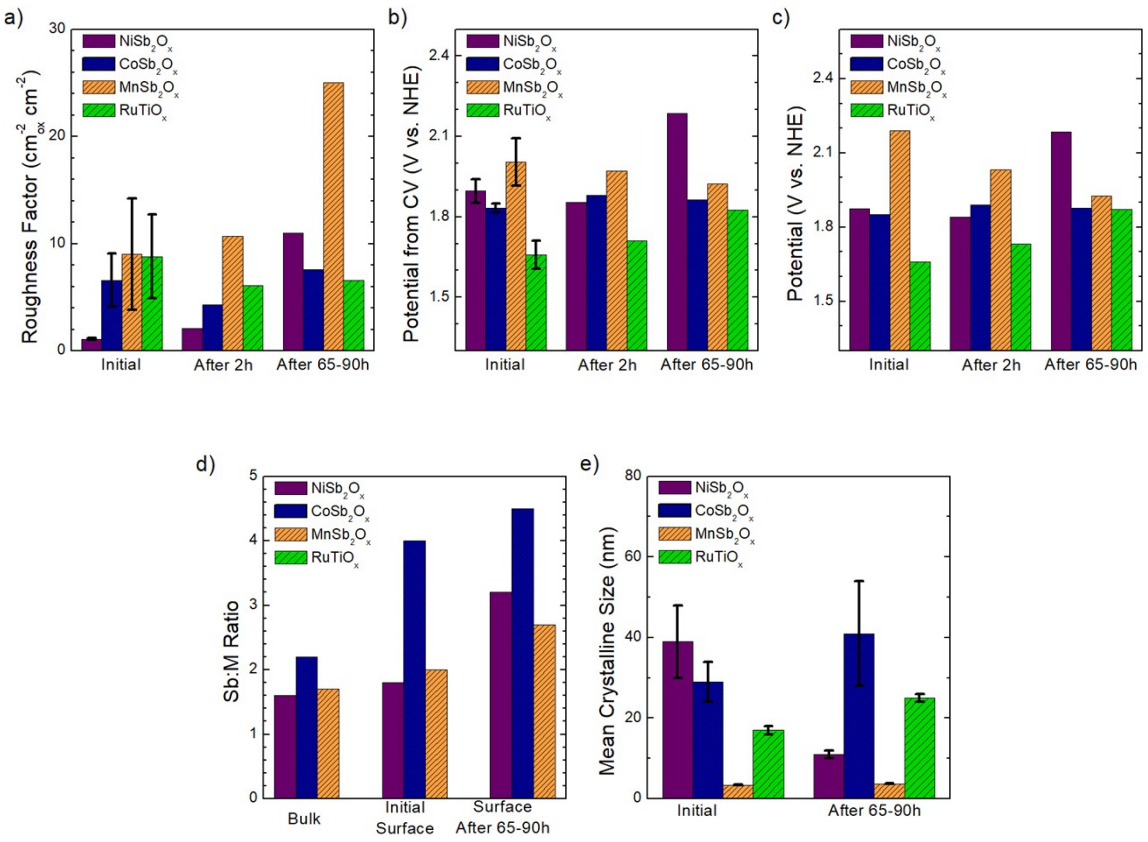

Figure S14. Summary of a) roughness factor, b) potential at 100 mA cm^{-2} from cyclic voltammetry, c) potential at 100 mA cm^{-2} from chronopotentiometry, d) bulk and surface composition, and e) mean crystalline size for $NiSb_2O_x$, $CoSb_2O_x$, $MnSb_2O_x$, and $RuTiO_x$. Final data is at 90 h for $CoSb_2O_x$, $MnSb_2O_x$, and $RuTiO_x$, and at 65 h for $NiSb_2O_x$.

Table S1. Catalyst loading of MSb_2O_x (M = Ni, Co, or Mn) films determined from ICP-MS measurements of MSb_2 films dissolved in 1.0 M H_2SO_4(aq).

Catalyst	M Loading (nmol cm^{-2})	Sb Loading (nmol cm^{-2})
$NiSb_2O_x$	483 ± 3	763 ± 5
$CoSb_2O_x$	375 ± 4	820 ± 5
$MnSb_2O_x$	417 ± 9	709 ± 8

Table S2. Potentials vs. NHE of MSb_2O_x films and $RuTiO_x$ determined from cyclic voltammetry data prior to galvanostatic operation at geometric current densities of 100 mA cm^{-2} in pH = 2.0, 4.0 M NaCl(aq). Roughness factors (RF) were determined from impedance data at 1.660 V vs. NHE. Faradaic efficiency (FE) towards the chlorine evolution reaction at a geometric current density of 100 mA cm^{-2} determined by iodometric titration. The faradaic efficiency experimental details such as the electrode areas, charge passed, amounts of Cl_2 expected, and amount of Cl_2 detected are included.

Catalyst	Potential at 100 mA cm^{-2} (V)	RF	FE Area (mm^{-2})	FE Charge Passed (C)	FE Cl_2 Expected (μmol)	FE Cl_2 Detected (μmol)	FE (%)
$NiSb_2O_x$	1.896 ± 0.045	1.1 ± 0.1	1.91	1.14	5.93	5.43, 5.83, 5.80	96.0 ± 3.7
$CoSb_2O_x$	1.833 ± 0.016	6.6 ± 2.5	3.49	2.09	10.8	10.3, 10.9, 10.5	97.4 ± 3.0
$MnSb_2O_x$	2.005 ± 0.088	9.0 ± 5.2	1.97	1.18	6.10	5.46, 5.47, 5.55	89.9 ± 0.8
$RuTiO_x$	1.659 ± 0.053	8.8 ± 3.9	11.76	7.05	36.5	35.0, 34.6, 34.3	94.8 ± 0.9

Table S3. Intrinsic Potential (E_i) vs. NHE at 1.0 mA cm^{-2} of ECSA and Tafel slope (b) of MSb_2O_x films and $RuTiO_x$ prior to and after 50 h of galvanostatic operation at 100 mA cm^{-2}. The Tafel slope was determined from a linear fit of a plot of η vs. $\log_{10}(J)$ between geometric current densities of 0.2 to 2.0 mA cm^{-2}. All Tafel slopes had an R-squared value greater than 0.99.

Catalyst	E_i at 0 h (V)	E_i at 50 h (V)	b at 0 h (mV dec^{-1})	b at 50 h (mV dec^{-1})
$NiSb_2O_x$	1.602 ± 0.018	1.911	94	131
$CoSb_2O_x$	1.652 ± 0.006	1.705	73	74
$MnSb_2O_x$	1.699 ± 0.036	1.789	110	110
$RuTiO_x$	1.460 ± 0.010	1.563	69	134

Table S4. Summary of XPS binding energies observed for MSb_2O_x samples before and after electrochemical operation and literature values for various M and Sb compounds.

Material	M $2p_{3/2}$ Binding Energy (eV)	Sb $3d_{5/2}$ Binding Energy (eV)	Reference
$NiSb_2O_x$ (before)	856.1 ± 0.1	540.4 ± 0.1	–
$NiSb_2O_x$ (after)	856.3 ± 0.1	540.5 ± 0.1	–
$CoSb_2O_x$ (before)	781.2 ± 0.1	540.6 ± 0.1	–
$CoSb_2O_x$ (after)	781.2 ± 0.1	540.3 ± 0.1	–
$MnSb_2O_x$ (before)	641.9 ± 0.1	540.2 ± 0.1	–
$MnSb_2O_x$ (after)	642.0 ± 0.1	540.3 ± 0.1	–
$NiCl_2$	856.77	–	[15]
$Ni(OH)_2$	855.80	–	[15]
$CoCl_2 \cdot (H_2O)_6$	782.1	–	[16]
$Co(OH)_2$	780.65	–	[6]
$MnCl_2$	642.0	–	[17]
Sb_2O_3	–	539.7	[8]
Sb_2O_4	–	540.3	[8]
Sb_2O_5	–	540.6	[8]

Table S5. Example of impedance data collected and ECSA determined for MSb_2O_x and $RuTiO_x$ films.

Catalyst	Area (cm^{-2})	R_s (Ω)	Q_0 $\mu F\ s^{(a-1)}$	a	R_{ct} (Ω)	C_{DL} (μF)	ECSA (cm^{-2})	RF
$NiSb_2O_x$	0.0179	110.2	6.87	0.714	343.3	0.341	0.0316	1.76
$CoSb_2O_x$	0.0282	29.29	2.87	0.912	396.6	1.15	0.1049	3.72
$MnSb_2O_x$	0.0179	153.1	21.0	0.704	1,522	1.81	0.1645	9.19
$RuTiO_x$	0.2030	16.91	49.9	0.871	8.790	14.9	1.355	6.67

References

1. H. Bisht, H.-T. Eun, A. Mehrtens and M. A. Aegerter, *Thin Solid Films*, 1999, **351**, 109-114.
2. I. A. Moreno-Hernandez, C. A. MacFarland, C. G. Read, K. M. Papadantonakis, B. S. Brunschwig and N. S. Lewis, *Energy Environ. Sci.*, 2017, **10**, 2103-2108.
3. N. Menzel, E. Ortel, K. Mette, R. Kraehnert and P. Strasser, *ACS Catal.*, 2013, **3**, 1324-1333.
4. S. Grazulis, D. Chateigner, R. T. Downs, A. F. Yokochi, M. Quiros, L. Lutterotti, E. Manakova, J. Butkus, P. Moeck and A. Le Bail, *J. Appl. Crystallogr.*, 2009, **42**, 726-729.
5. J. D. Donaldson, A. Kjekshus, D. G. Nicholson and T. Rakke, *Acta Chem. Scand. A*, 1975, **29**, 803-809.
6. M. C. Biesinger, B. P. Payne, A. P. Grosvenor, L. W. M. Lau, A. R. Gerson and R. S. C. Smart, *Appl. Surf. Sci.*, 2011, **257**, 2717-2730.
7. M. C. Biesinger, B. P. Payne, L. W. M. Lau, A. Gerson and R. S. C. Smart, *Surf. Interface Anal.*, 2009, **41**, 324-332.
8. R. Izquierdo, E. Sacher and A. Yelon, *Appl. Surf. Sci.*, 1989, **40**, 175-177.
9. J. I. Partanen and A. K. Covington, *J. Chem. Eng. Data*, 2009, **54**, 208-219.
10. C. C. McCrory, S. Jung, J. C. Peters and T. F. Jaramillo, *J. Am. Chem. Soc.*, 2013, **135**, 16977-16987.
11. M. Wohlfhart-Mehrens and J. Heitbaum, *J. Electroanal. Chem.*, 1987, **237**, 251-260.
12. in *Standard Methods For the Examination of Water and Wastewater*, DOI: 10.2105/smww.2882.078.
13. C. E. Finke, S. T. Omelchenko, J. T. Jasper, M. F. Lichterman, C. G. Read, N. S. Lewis and M. R. Hoffmann, *Energy Environ. Sci.*, 2019, **12**, 358-365.
14. M. Jiang, H. Wang, Y. Li, H. Zhang, G. Zhang, Z. Lu, X. Sun and L. Jiang, *Small*, 2017, **13**.
15. M. C. Biesinger, L. W. Lau, A. R. Gerson and R. S. Smart, *Phys. Chem. Chem. Phys.*, 2012, **14**, 2434-2442.
16. D. G. Brown and U. Weser, *Z. Naturforsch. (B)*, 1979, **34**, 1468-1470.
17. A. Aoki, *Jpn. J. Appl. Phys*, 1976, **15**, 305-311.